Egyptian Journal of Chemistry

http://ejchem.journals.ekb.eg/

Eco-friendly synthesis, docking study, pharmacokinetics studies, and anti-proliferative evaluation of pyrimidine derivatives as dual Topoisomerase II and HSP90 inhibitors

Eman S. Tantawy[a], Wesam S. Shehab[a], Omnia M. Abo Elenin[a], Mohamed G. Assy[a], Doaa A. Elsayed[a]*

[a]Department of Chemistry, Faculty of Science, Zagazig University, Zagazig 44519 Egypt.

Abstract

Manganese oxide nanoparticles (Mn3O$_4$-NPs) were used as a heterogeneous nano catalyst in this work to create a novel series of pyrimidine derivatives in an ecologically acceptable manner. Simple and easily accessible starting ingredients were used in a one-pot, multicomponent reaction as part of the synthetic approach. Co-precipitation was used to create the Mn3O$_4$-NPs, and XRD and SEM were used to verify their crystalline structure and nanoscale shape. FT-IR, UV-visible, ^{1}H NMR, and elemental CHN analysis were among the spectroscopic methods used to establish the structural identity of the synthesized pyrimidine derivatives. The MTT test was used to assess the newly synthesized compounds' anticancer potential in vitro against human cancer cell lines. The compounds' selectivity was also evaluated by measuring their cytotoxicity to normal cells. Several derivatives of the investigated drugs showed low IC$_{50}$ values and strong antiproliferative action. Molecular docking experiments were conducted against Topoisomerase II and Heat Shock Protein 90 (HSP90), two important cancer-related enzymes, in order to investigate the molecular interactions at the target level. The possible mechanism of anticancer activity was supported by the docking studies, which showed substantial binding affinities and advantageous interactions with important active site residues.

Keywords: pyrimidines, Nanoparticles, anti-proliferative, (Mn$_3$O$_4$-NPs), Topoisomerase II, HSP90 inhibitors, molecular docking

1.   Introduction

The complicated genesis of cancer and the well-known propensity of tumor cells to become resistant to standard treatments are major reasons why it continues to be a serious worldwide health concern. A definitive and widely accepted cancer treatment is still elusive, despite tremendous advancements in biochemistry, molecular oncology, and drug design [1-4]. Tumor heterogeneity and acquired resistance to current therapeutic drugs are frequently blamed for the ongoing increase in cancer incidence, which fuels the ongoing search for novel chemotherapeutic approaches that may target several signaling pathways at once [5-9].

In response to these therapeutic challenges, multicomponent reactions (MCRs) have gained attention as effective, environmentally friendly synthetic pathways that can minimize the need for laborious purification steps by producing structurally diverse libraries of biologically active compounds in a single step [10-12]. The Biginelli reaction is one of the most useful synthetic methods for producing 1,2,3,4-tetrahydropyrimidine (THPM) derivatives, which have been shown to have a wide range of pharmacological activities, such as anti-inflammatory, antiviral, anticancer, and antimicrobial qualities [13-15].

Strong anti-proliferative effects against a variety of cancer cell lines have been shown by compounds based on THPM. More structural research is required since recent studies have demonstrated that substitution patterns at particular locations of the THPM scaffold have a considerable impact on their biological activity [16-20].

THPM analogues with notable cytotoxicity against liver (HEPG-2) and breast (MCF-7) cancer cells have been produced and described by our research team in the past [21, 22]. To enhance the therapeutic potential of THPM analogues, nanotechnology has been integrated into drug design, particularly through the application of metal oxide nanoparticles (e.g., TiO$_2$, ZnO, Mn$_3$O$_4$) as heterogeneous catalysts, which not only accelerate reaction rates but also offer improved selectivity and environmental compatibility [23-26]. Among these, Mn$_3$O$_4$ nanoparticles have emerged as efficient and green catalysts in organic transformations, including the synthesis of anticancer heterocycles [27, 28], (Figure 1).A new series of

tetrahydropyrimidine analogues was logically designed and synthesized in this work employing Mn3O₄ nanoparticles as a catalyst. Computational investigations led the molecular design, with the THPM core undergoing strategic alterations to modulate its hydrophobic, steric, and electrical characteristics. To improve binding affinity to important oncogenic enzymes like Topoisomerase II and HSP90, which are essential for DNA replication and the stress response in cancer cells, bioisosteric replacements and substituents with pharmacophoric potential were added [29, 30].

The hybrid strategy that combines structure-based medication design, environmentally friendly nanocatalysis, and in vitro/in silico biological assessments is what makes this study innovative. As demonstrated by molecular docking simulations using MOE (ver. 2022), this comprehensive technique not only produced THPM analogues with potential cytotoxic characteristics but also offered important insight into their binding interactions with therapeutic targets at the atomic level. By offering a green synthetic approach and producing structurally optimized pyrimidine derivatives with improved biological activity and target specificity, this study makes a substantial contribution to the field of anticancer drug development and may open the door for the preclinical development of potent, low-toxicity anticancer drugs.
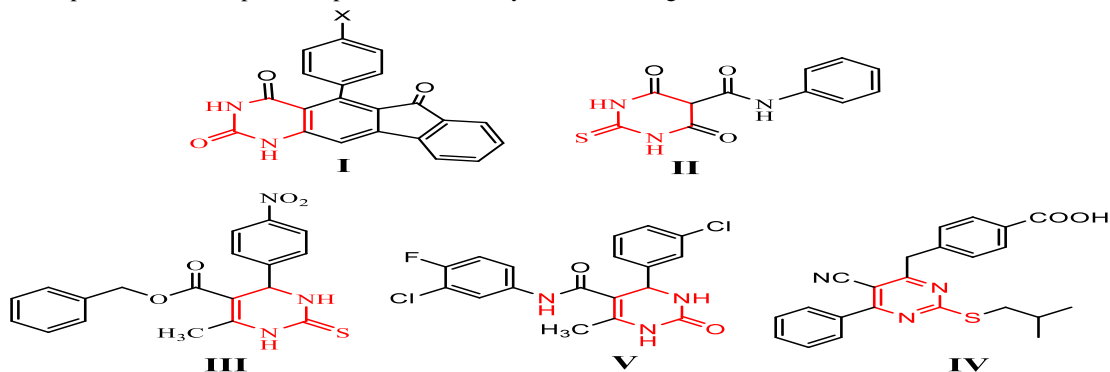
Figure 1. pyrimidine derivatives as anti-proliferative agents against different cancer cell lines.

2. Experimental Section

2.1 Materials and Methods

The desired compounds were synthesized with high-quality materials. Sigma-Aldrich (Taufkirchen, Germany) furnished the chemicals (ethyl cyanoacetate 99%, thiourea 99.5%, 4-nitrobenzaldehyde 99%, and ethyl iodide. Sigma-Aldrich Company provided solvents (99.8% ethanol, pyridine, acetic anhydride, and 99.7% acetic acid). (HR-TEM) [JEM-2100, Tokyo, Japan] was used to investigate the nature and crystallinity of the nanoparticles. Infrared (IR) spectra, acquired using potassium bromide (KBr), were performed using a Shimadzu FT-IR 8101 PC infrared spectrophotometer. Using a BRUKER 400 MHz spectrometer, carbon-13 nuclear magnetic resonance (^{13}C NMR) and proton nuclear magnetic resonance (^{1}H NMR) spectra were obtained at 100 MHz and 400 MHz, respectively. Hertz (Hz) is used to describe coupling constants (J), and the delta (δ) scale is used to report chemical shifts in parts per million (ppm) wherein the internal standard was tetramethylsilane (TMS). Elemental analysis was performed with a Perkin Elmer 240 instrument. Molecular docking scores were calculated and analyzed using the 2022 version of the Molecular Operating Environment (MOE) software.The human cell lines (MCF-7, HEPG-2) were acquired from ATCC through the Holding Company for Biological Products and Vaccines (VACSERA) in Cairo, Egypt. For comparison, doxorubicin was provided as the standard anticancer agent. The reagents included fetal bovine serum (GIBCO, UK), RPMI-1640 medium, and DMSO and MTT (Sigma Co., St. Louis, USA).

2.2 Preparation of Mn₃O₄ nanoparticles

The precipitation method was used to produce Mn3O₄ nanoparticles. Briefly, 10 g of manganese (II) nitrate (Mn(NO₃)₂.4H₂O, 99%) was dissolved in 0.5 L distilled H₂O to form a 0.4 M solution. A (2 M) NaOH solution was added dropwise to the manganese (II) nitrate solution under strong magnetic stirring until the pH became 10 at room temperature. The solid precipitation looks white for a short period at this pH before becoming brown. After 2 h of chemical reaction, the precipitate was allowed to simmer overnight. After repeatedly rinsing the brownish precipitate with distilled water to get rid of

_____

Egypt. J. Chem. **68,** SI: Z. M. Nofal (2025)

_____

extra NaOH, it was filtered and dried for 4 h at 100 °C. The clean dried precipitate was preserved in a desiccator until it was used.

2.3 Characterization

A variety of methods are used to identify the processed Mn_3O_4-NPs produced by the precipitation technique. The crystallinity of the material was studied using XRD on a [Bruker D_8 advance diffractometer, Germany] using Cu Kα radiation (λ = 1.5406 Å). A field emission scanning electron microscope (FE-SEM, Quanta FEG-250, Netherlands) and energy dispersive X-ray analysis (EDX) were utilized to investigate the size and surface structure of the generated Mn_3O_4-NPs. A thin layer of gold was applied to the surface using a [S150A sputter coater, Edwards, England] set to 0.1 Torr, vacuum, 50 mA current, and 1.2 kV voltage to provide sample scanning. Additionally, a high-resolution transmission electron microscope (HR-TEM, JEM-2100 Joel model, 200 kV working voltage, Japan) was used to examine the characteristics and crystallinity of nanoparticles. For microscopy analysis, the aqueous dispersion of the particles was drop-casted onto copper grid that had been coated with carbon and left to dry at room temperature.

2.4 Chemistry

Traditional Method

A mixture of 0.01 mol of 4-nitrobenzaldehyde (1.51g), 0.01 mol of thiourea (0.76g), 0.01 mol of ethyl cyanoacetate (1.13g), and 0.03 mol of anhydrous potassium carbonate (4.14g) in 50 mL of Abs. EtOH was magnetically stirred under reflux for 12 h. After the reaction time, the reaction mixture cooled down, and the resulting precipitate was liquefied in H_2O and counterbalanced with dilute HCl. Compound 1 was produced as white crystals after the solid was filtered out, splashed with 95% EtOH, and recrystallized from EtOH: (yield: 70%), m.p. 270-272°C. [lit: 276-278°C][31].

Nano catalytic Method

The equimolar quantities of 0.01 mol of 4-nitrobenzaldehyde (1.5 g), 0.01 mol of thiourea (0.76 g), 0.01 mol of ethyl cyano-acetate (1.13g), or 0.01 mol of acetylacetone (1 g) or 0.01 mol of ethyl acetoacetate (1.3 g) in 50 mL of abs. EtOH in the presence of (0.03 g) nano Mn_3O_4 was magnetically stirred under reflux for 5h. The solid product was clarified and subsequently recrystallized from ethanol, yielding compounds **1, 2**, and **3**, respectively.

6-(4-Nitrophenyl)-4-oxo-2-thioxo-1,2,3,4-tetrahydropyrimidine-5-carbonitrile (1):

White crystals. (Yield: 95%) m.p. 274-276°C [lit: 276-278°C]. IR (KBr, ν, cm^{-1}): 3554, 3466 and 3420 (2 NH str), 2215 (C≡N), 1692 (C=O amide), 1267(C=S). ^{1}H-NMR (DMSO-d_6, 400 MHz): δ= 8.50 (s, 1H, NH, exchangeablewith D_2O), 8.16-8.18 (d, 2H, *J=8* Hz, 2 Ar-H), 8.23-8.25 (d, 2H, *J=8*, 2 Ar-H), 10.17 (s, 1H, NH, exchangeable with D_2O). ^{13}C-NMR (DMSO-d_6, 100 MHz) δ (ppm) = 63.23, 107.18, 115.41, 124.62, 132.13, 137.74, 149.71, 153.16, 161.61, 184.2. Anal. Calcd. For $C_{11}H_6N_4O_3S$ (274.25): C, 48.17; H, 2.21; N, 20.43. Found; C, 48.15; H, 2.18; N, 20.40.

1-(4-Methyl-6-(4-nitrophenyl)-2-thioxo-1,2-dihydropyrimidin-5-yl)ethan-1-one (2):

Buff powder: (yield: 20%), m.p: (160 -162°C). IR (KBr, ν, cm^{-1}): 3504, 3435 (NH), 2855 (CH- aliphatic) 1707 (C=O). ^{1}H-NMR (DMSO-d_6, 400 MHz): δ= 2.00 (s, 3H, CH_3), 2.51 (s, 3H, $COCH_3$), 8.16-8.18 (d, 2H, *J=8* Hz, 2 Ar- H), 8.38-8.40 (d, 2H, *J=8,*2Ar-H), 10.16 (s, 1H, NH, exchangeable with D_2O). Elemental Analysis: C, 53.97; H, 3.83; N, 14.52; O, 16.59; S, 11.08 Anal. Calcd. for $C_{13}H_{11}N_3O_3S$ (289.3): C, 53.97; H, 3.83; N, 14.52. Found; C, 53.95; H, 3.80; N, 14.54.

Ethyl 4-methyl-6-(4-nitrophenyl)-2-thioxo-1,2,3,4-tetrahydropyrimidine-5-carboxylate (3):

Yellow solid (yield: 15%), m.p (124-126°C). IR (KBr, ν, cm^{-1}): 3434, 3402 (2 NH), 2853(CH -aliphatic), 1724 (C=O ester), ^{1}H-NMR: δ, ppm (DMSO-d_6, 400 MHz): 0.95-0.99 (t, 3H, *J=7.2 Hz* OCH_2CH_3), 2.52 (s, 3H, CH_3), 3.95 (q, 2H, OCH_2CH_3), 4.89 (s,1H,CH), 7.61-7.63 (d, 2H, *J = 8 Hz*, 2 Ar-H), 8.19-8.21 (d, 2H, *J =8 Hz*, 2 Ar-H), 8.60 (s, 1H, NH, exchangeable with D_2O). 8.89 (s, 1H, NH, exchangeable with D_2O). ^{13}C-NMR (DMSO-$d6$, 100 MHz) δ (ppm) = 14.32, 27.7, 54.34, 54.66, 60.83,

_____

_____

78.43, 129.75, 130.29, 147.46, 147.66, 163.49, 175.81, 181.27. Anal. Calcd. For $C_{14}H_{15}N_3O_4S$ (321.4): C, 52.33; H, 4.71; N, 13.08. Found; C, 52.30; H, 4.73; N, 13.10.

4-Imino-8-(4-nitrophenyl)-2,6-dioxo-3,4-dihydro-2H,6H-pyrimido[2,1-b][1,3]thiazine-carbonitrile (4):

 Compound **4** was synthesized by reacting 2 mmol of compound **1** (0.548 g) with 2 mmol of ethyl cyanoacetate (0.226 g) in 20 mL of dioxane followed by heating the reaction mixture for 6 h under reflux. After concentration, the precipitate was formed from the reaction mixture after cooling to room temperature. The resulting precipitate was then collected and recrystallized from EtOH to produce compound **4** (m.p. 150-152°C, 54% yield), IR (KBr) spectrum, ν, cm⁻¹: 3452, 3398 (NH), 2210 (C≡N), 1719, 1695 (2C=O thiazine, pyrimidine). ¹H-NMR (DMSO-d_6, 400 MHz), δ (ppm): 4.33(s, 2H, CHmethylene), 8.24-8.26 (d, 2H, *J=8 Hz*, 2 Ar-H), 8.39-8.41 (d, 2H, J=8, 2 Ar-H), 8.55 (s, 1H, NH, exchangeable with D_2O). ¹³C-NMR (DMSO-d_6), δ(ppm): 14.46, 63.21, 107.16, 115.40, 124.63, 132.15, 137.75, 149.72, 153.15 and 161.61. Anal. Calcd for $C_{12}H_8N_6O_3S$ (316.3): C, 45.57; H, 2.55; N, 26.57. Found; C, 45.60; H, 2.59; N, 26.60.

7-(4-Nitrophenyl)-3,5-dioxo-2,3-dihydro-5H-thiazolo[3,2-a]pyrimidine-6-carbonitrile(5): Compound **5** was synthesized by reacting 0.001 mol of compound **1** (0.3 g) with 0.001 mol of chloroacetic acid (0.1 g), and 0.004 mol of anhydrous sodium acetate (0.18 g) in a mixture of acetic anhydride (2 mL) and glacial acetic acid (10 mL). Followed by heating the reaction mixture for 3 h under reflux and then poured into icy water. Compound **5** was then obtained by filtering and recrystallizing the resultant precipitate from benzene. Yield (53%), m.p. 140-142°C. IR (KBr) spectrum, ν, cm⁻¹: 2220 (C≡N), 1682 (2C=O thiazole and pyrimidine). ¹H NMR (DMSO-d_6), δ (ppm): 4.35 (s, 2H, CH_2 thiazole), 8.24-8.26 (d, 2H, *J=8 Hz*, 2 Ar-H), 8.40-8.42 (d, 2H, *J=8*, 2Ar-H). Anal. Calcd for $C_{13}H_6N_4O_4S$ (314.3); C, 49.68; H, 1.92; N, 17.83. Found; C, 49.64; H, 1.96; N, 17.87.

7-(4-Nitrophenyl)-5-oxo-1,2,3,5-tetrahydroimidazo[1,2-a]pyrimidine-6-carbonitrile (6):

A solution of compound **1** (4 mmol, 1 g) and ethanolamine (4 mmol, 0.22 g) in 10 mL of isopropyl alcohol was refluxed for 6 h. The reaction mixture was concentrated, then put into icy water and acidified with 0.1 M HCl. After filtering and recrystallizing the resultant precipitate from benzene, compound **6** an orange solid was obtained. Yield (43%), m.p.112-114°C, IR (KBr) spectrum, ν, cm⁻¹: 3405, 3362 (NH), 2215 (C≡N), 1690 (C=O amide). ¹H NMR (DMSO-d_6), δ (ppm): 3.42 (m, 2H, CH_2 imidazole), 4.37 (m, 2H, CH_2 imidazole), 8.39-8.41 (d, 2H, *J=8*Hz, 2 Ar-H), 8.53-8.55 (d, 2H, *J=8*, 2 Ar-H), 10.27 (s, 1H, NH, exchangeable with D_2O). ¹³C NMR (DMSO-d_6), δ(ppm): 39.78, 43.10, 63.21, 107.16, 115.39, 124.14, 129.40, 140.54, 160.92, 166.02. Anal. Calcd for $C_{13}H_9N_5O_3$ (283.2) C, 55.13; H, 3.20; N, 24.73; Found; C, 55.15; H, 3.22; N, 24.70.

2-(Ethylthio)-4-(4-nitrophenyl)-6-oxo-1,6-dihydropyrimidine-5-carbonitrile (7):

An equimolar mixture of compound **1** (0.004 mmol, 1 g) and ethyl iodide (0.004 mmol, 0.624 g) in 20 ml of EtOH, with anhydrous sodium acetate (0.004 mmol, 0.33 g), followed by heating for 16 h under reflux. After reaction time, the mixture was transferred into the ice bath. Compound **7** is the orange solid that was obtained by filtering, drying, and recrystallizing the precipitate from EtOH. Yield (35%), m.p 120-122°C. IR (KBr) spectrum, ν, cm⁻¹: 3370 (NH), 2932 (CH aliphatic), 2213 (C≡N), 1692 (C=O). ¹H NMR (DMSO-d_6): δ (ppm): 1.27 (t, 3H, -CH_2CH_3), 2.44 (q, 2H, -CH_2CH_3), 7.82-7.84 (d, 2H, *J=8*, 2 Ar-H), 8.05-8.16 (d, 2H,*J=8*,2 Ar-H), 11.52 (s, 1H, NH, exchangeable with D_2O). Anal. Calcd for $C_{14}H_{13}N_3O_2S$ (287): C, 58.53; H, 4.52; N, 14.63. Found: C, 58.26; H, 4.32; N, 14.83.

1-Acetyl-6-(4chloro-3-nitrophenyl)-4-oxo-2-thioxo-1,2,3,4-tetrahydropyrimidine-5-carbonitrile (8):

The reaction mixture contained compound **1** (4 mmol, 1 g), acetic anhydride (15 mL), and a few drops of pyridine followed by heating for 8h under reflux. After the reaction time, the reaction mixture was neutralized by adding dropwise dilute HCl (0.1M) resulting in the formation of a precipitate. Compound **8** was obtained as a dark brown precipitate by filtering, drying, and recrystallizing the resulting precipitate from methanol. Yield (60%), m.p. 136-138°C; IR (KBr) spectrum, ν, cm⁻¹: 3399 (NH), 2221 (C≡N), 1742, 1692 (2C=O). ¹H NMR (DMSO-d_6): δ (ppm): 1.91 (s, 3H, CH_3), 7.75-8.40 (m, 4H, 4Ar-H), 12.66 (s, 1H, NH exchangeable with D_2O). ¹³C NMR (DMSO-d_6), δ (ppm): 21.54, 65.18, 115.80, 124.57, 129.78, 132.97, 141.81,

_____

_____

148.39, 167.52, 172.52. Analysis Calcd. for $C_{13}H_8N_4O_4S$ (316.3): C, 49.37; H, 2.55; N, 17.71; Found C, 49.40; H, 2.53; N, 17.70.

2.5 Biology

The MTT assay was employed with the previously described cell lines to examine the inhibitory activity of synthesized substances on cell proliferation. The mechanism of action of this colorimetric assay is to demonstrate how mitochondrial succinate dehydrogenase transforms yellow tetrazolium bromide (MTT) into a purple formazan derivative in living cells. Cell lines were cultivated in RPMI-1640 media supplemented with 10% fetal bovine serum. In an incubator with 5% CO_2, the culture had been kept at 37°C and treated with 100 μg/mL of streptomycin and 100 units/mL of penicillin. A 96-well plate was filled with 1.0×10^4 cells per well, and the cells were incubated with 5% CO_2 at 37°C for 48 h. The cells were incubated for a further 24 hours after being exposed to different chemical concentrations. After the treatment, each well received 20 μL of MTT solution (5 mg/mL) followed by a 4-hour incubation period. Next, 100 μL of DMSO was added to each well for dissolving the purple-colored formazan crystals. The ELx800 Microplate reader (USA) was utilized to monitor and record the colorimetric change at 570 nm. The relative viability of cells was calculated using the formula (A570 of treated samples / A570 of untreated samples) × *100%* [32, 33].

2.6 Molecular docking simulation

Docking was performed according to the previously published literature[34]. Topoisomerase II (PDB ID: 1QZR)[35] and HSP90 (PDB ID: 1YET)[36]. The MOE 2022 program was used to create crystallographic structures for MD by eliminating ligands, adding hydrogens, and optimizing energy. The energy-optimized structure acted as the docking receptor. The catalytic sites of Topo II and HSP90 were identified using the MOE site-finding technique. The 2D structures of the synthesized compounds were created using ChemBioOffice, and then they were constructed in MOE 2022 utilizing fragment libraries. The MMFF94x force field in MOE was used to reduce energy consumption. To study and examine the interactions between ligands and the Topo II and HSP90 binding sites, docking was done using particular parameters. The parameters were Triangle Matcher for placement, Retention: 2, and Force Field for refining[37]

3. Results and Discussion

3.1. Characterization of Mn_3O_4 nanoparticles
XRD Analysis

Figure 2 displays the diffraction peaks of the huminite structure (Mn_3O_4 nanoparticles) in the XRD pattern of the crystalline sample. When the standard value and the measured diffraction peak positions were compared, it was discovered that they agreed with [(JCPDS 24-0734)], which corresponds to the tetragonal single phase of (Mn_3O_4 nanoparticles). The tetragonal unit cell lattice parameters were (a = b = 5.76 Å and c = 9.46 Å), which were consistent with previous findings. The XRD investigation imparts no additional impurity peaks, oblique the lack of any other manganese oxide formulation.
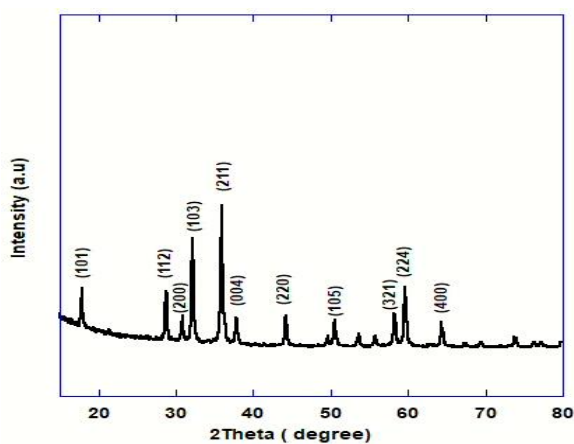
Figure 2. XRD pattern of Mn_3O_4-NPs

_____

_____

3.2. Morphological and elemental analyses

The size, shape, and crystallinity of Mn$_3$O$_4$ nanoparticles were investigated using FE-SEM and TEM measurements. An FE-SEM image of Mn$_3$O$_4$-NP is seen in Figure 3a. The particles were found to be uniformly sized, significantly agglomerated, and either spherical or cubic in shape. This observation is consistent with the reported SEM results[38]. The high purity of the synthesized sample was confirmed by the EDX results in Figure 3b, which showed the presence of just Mn and O elements. The manganese oxide nanostructure (Mn$_3$O$_4$) nanoparticles are shown in a typical TEM image in Figure 3c demonstrating the highly crystalline structure of synthesized Mn$_3$O$_4$NPs [39]. Particle sizes in the sample were likely between 15 and 70 nm, with the majority of the particles being cubic and a small number of spherical structures. The selected area electron diffraction (SAED) pattern displayed in Figure 3d indicates that the Mn$_3$O$_4$ nanoparticles are polycrystalline[40]
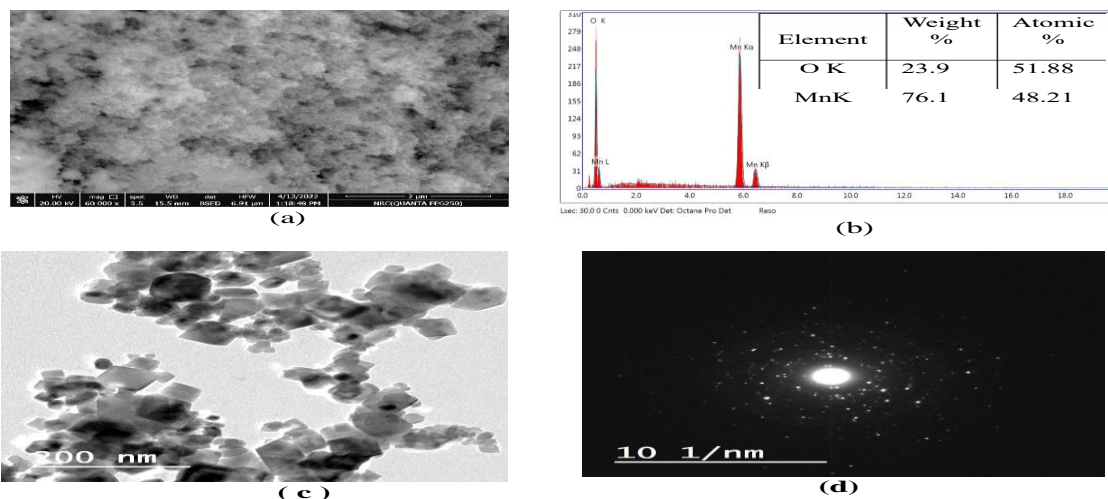

Figure 3. SEM image (scale bar: 2µm), (b) EDX Spectrum, (c) TEM image (scale bar:200nm), and (d) the selected area electron diffraction (SAED) pattern of synthesized Mn$_3$O$_4$

3.2. Chemistry

The synthesis of 2-thiopyrimidines 1 was accomplished through a one-pot, three-component Biginelli reaction. Two methods were used to produce 6-(4-Nitrophenyl)-4-oxo-2-thioxo-1,2,3,4-tetrahydropyrimidine-5-carbonitrile (compound 1). The traditional method involves reacting 4-nitrobenzaldehyde with thiourea and ethyl cyanoacetate in ethanol under reflux conditions, with anhydrous potassium carbonate as the catalyst, to procure compound 1.

This is the precedent method used that was described in a previous work Scheme (1)[31].
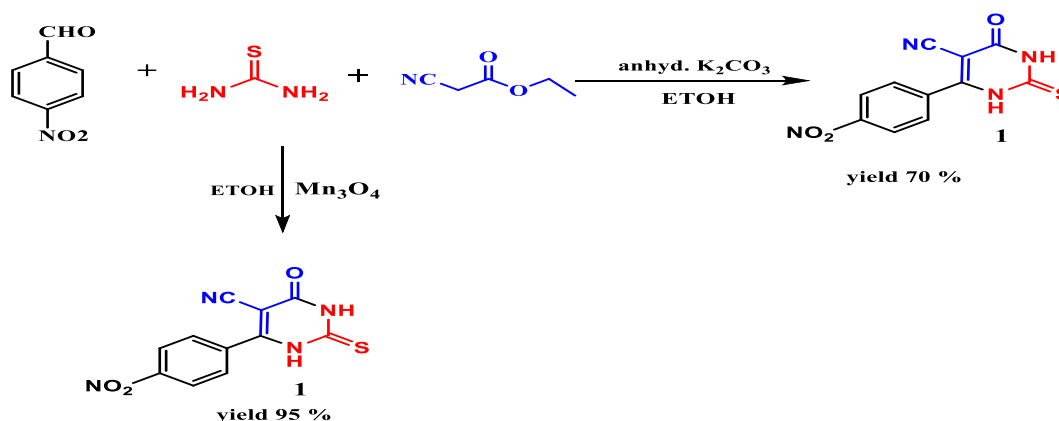
Scheme (1). synthesis of 6-(4-Nitrophenyl)-4-oxo-2-thioxo-1,2,3,4-tetrahydropyrimidine-5 carbonitrile 1

_____

_____

The caliber method involves reacting 4-nitrobenzaldehyde with thiourea and ethyl cyanoacetate in the presence of three different Nanocatalysts (TiO$_2$, ZnO, and Mn$_3$O$_4$), using ethanol under reflux conditions. The reaction catalyzed by Mn$_3$O$_4$nanoparticles achieved a significantly higher yield, reaching 95%, with a shorter reaction time compared to the traditional methods. This approach demonstrated improved yields over those reported for conventional techniques[41]. Data are summarized in Table 1.

Table (1). Optimization of different nanoparticles and their effects on yield of 6-(4-Nitrophenyl)-4-oxo-2-thioxo-1,2,3,4-tetrahydropyrimidine-5-carbonitrile 1

| Entry	Solvent	Catalysis(mol)	Temp©	Time(h)	Yield(%)	Ref.
1	EtOH	No catalyst	reflux	9	No yield	This work
2	EtOH	K$_2$CO$_3$	reflux	12	70%	[31]
3	EtOH	Mn$_2$O$_3$	reflux	5	95%	This work
4	EtOH	TiO$_2$	reflux	4	42%	This work
5	EtOH	ZnO	reflux	4	62%	This work
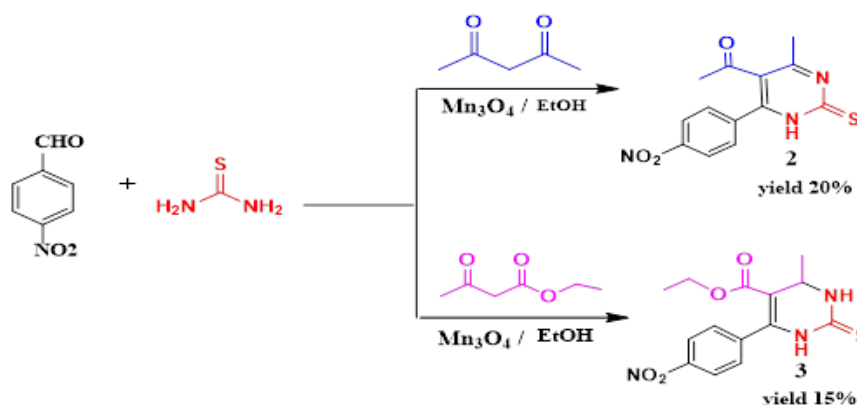
Scheme (2). Synthesis of 2-thio pyrimidine derivtives.

As shown in Scheme (2), derivatives of 2-thiopyrimidine were synthesized through a one-pot three-component reaction of (4-nitrobenzaldehyde), thiourea, and/or active methylene compounds namely: acetylacetone and ethyl acetoacetate in the occurrence of Mn$_3$O$_4$ nanoparticles (Mn$_3$O$_4$-NPs) as a catalytic amount in ethanol were refluxed for appropriate time. Compound **1** is the most with optimal reaction conditions with a higher yield (95%). In comparison, compound **2** shows a yield of just 20%, while compound **3** has a yield of 15%. Scheme (3) presents a suggested mechanism for the development of compound **1** in the presence of catalytic Mn$_3$O$_4$ nanoparticles.

Using ^{13}C-NMR, ^{1}H-NMR, and FTIR spectroscopy, the structure of compound **1** was characterized. The FTIR spectrum displayed the absorption band at 1276 cm^{-1} for the C=S group and at 1692 cm^{-1} related to the C=O group, while a band at 2181 cm^{-1} for the CN group, and absorption bands at 3554, 3466, and 3420 cm^{-1} that related to two NH groups. The ^{1}H NMR spectrum showed doublet signals at 8.16-8.18 and 8.23-8.25 ppm, attributed to two aromatic hydrogen atoms, and singlet signals at 8.50 and 10.17 ppm, demonstrating the presence of two NH groups. The ^{13}C NMR spectrum revealed SP and SP^2 carbons associated with the C≡N, C=O, and C=S functional groups at chemical shifts of 115.41, 161.61, and 184.20 ppm, respectively.

The structure of compounds **2** and **3** were determined using IR, ^{1}H NMR, and ^{13}C NMR analyses. The ^{1}H NMR spectrum of compound 2 displayed singlet signals at 2.52, 3.39, and 10.16 ppm which corresponded to –CH$_3$, –COCH$_3$, and NH groups, respectively, with aromatic protons appearing in the 8.16-8.40 ppm range. Compound 3 was identified by the existence of an ethyl ester group, evident from the C=O ester absorption in the IR spectrum, and ethyl group signals as triplet and quartet at 0.99 and 3.95 ppm, respectively, along with a singlet at 2.52 ppm for –CH$_3$ in the ^{1}H NMR spectrum.

_____

_____

The pyrimidothiazine derivative **4** was synthesized by reacting ethyl cyanoacetate with pyrimidine thione**1** in refluxing dioxane. This reaction most likely starts with the nucleophilic thiol group attacking the ester carbonyl group, leading to ethanol elimination and subsequent cyclization. Alternatively, thiazolo-pyrimidine derivatives 5 were synthesized by reacting compound **1** with chloroacetic acid. Using FTIR spectroscopy, the chemical structures of compounds 4 and **5** were confirmed. The results indicated the presence of carbonyl absorption bands at 1719 and 1720 cm^{-1}, which are suggestive of the oxo-thiazolo and oxo-thiazine rings, and the absence of the NH absorption band. Furthermore, the ^{1}H NMR spectrum for compound **4** revealed singlet signals at 4.33 and 4.35 ppm corresponding to (COCH$_2$) (Scheme 4). Compound **6** was prepared by reacting compound 1 with ethanolamine in isopropyl alcohol (Scheme 4). Alkylation of compound 1 using ethyl iodide at a 1:1 molar ratio in the presence of sodium acetate, yielding S-alkylated product **7**. The ^{1}H NMR spectrum of compound **7** revealed signals at $\delta = 1.27$ and 3.44 ppm, indicating the presence of CH$_2$ and CH$_3$ protons, which corroborates its proposed structure. Ultimately, compound **1** was heated with acetic anhydride in the presence of pyridine, leading to the formation of the 1-acetyl derivative. The ^{1}H NMR spectrum of compound 8 exhibited a signal at $\delta = 1.91$ ppm, corresponding to the acetyl CH$_3$ group. The ^{13}C NMR spectrum of compound **8** also assumes further structural information.
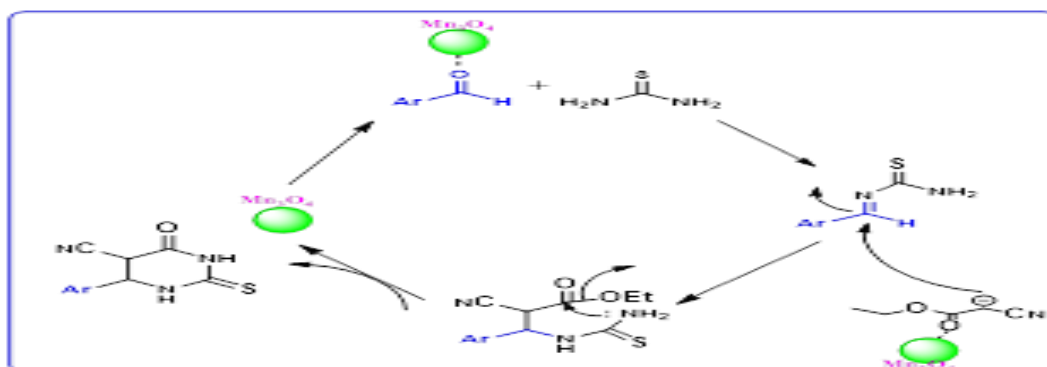
Scheme (3). General mechanism pathway for formation of tetrahydropyrimidine-5-carbonitrile (1).
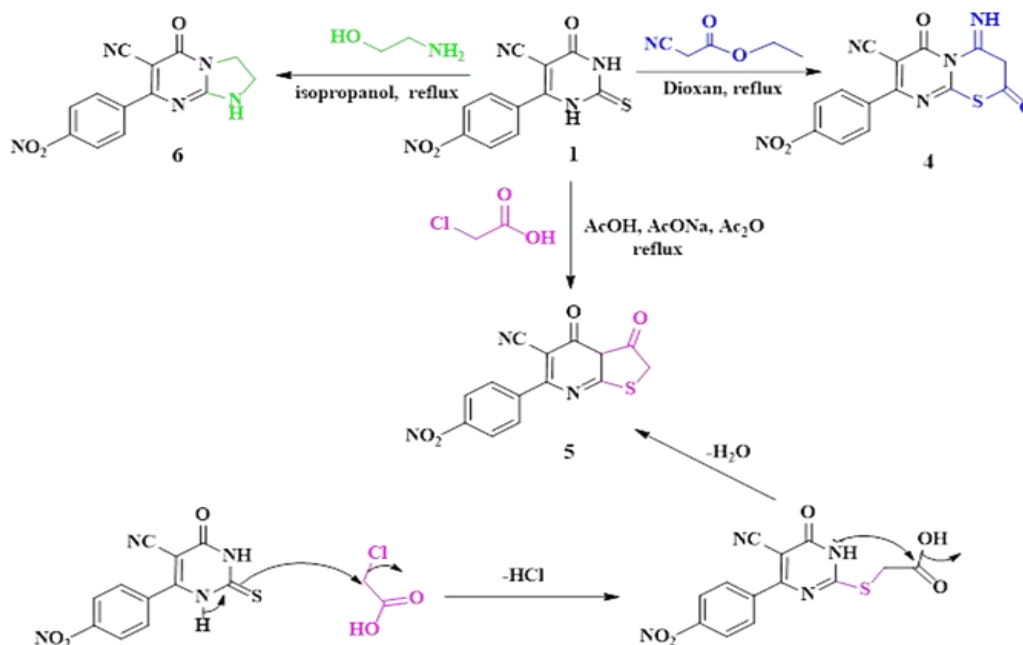
Scheme (4). synthesis of fused pyrimidine derivatives

_____

_____

Scheme (5). Synthesis of isolated pyrimidine derivatives
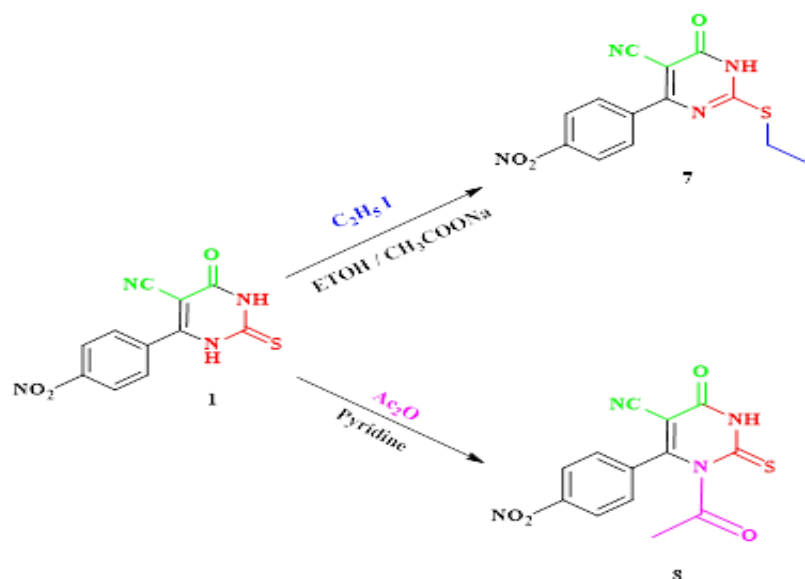
3.3. Biology

We evaluated the anticancer activity of all synthesized chemical products against Mammary gland breast cancer (MCF-7) and Hepatocellular carcinoma (HEPG-2) cell lines. The results, presented in Table 2, reveal that compounds **7** and **8** exhibit notable cytotoxic effects against both MCF-7 and HEPG-2 cells, with varying degrees of benefit compared to conventional doxorubicin, as illustrated in Figure 4.

Compounds **7** and **8** exhibit the highest effectiveness against the HEPG-2 cell line as demonstrated by Figure 4A, with IC_{50} (Table 2) values of 13.43 and 29.65 μM, respectively. In contrast, other compounds show lower cytotoxicity. Moreover, Figure 4B indicates that compounds **7** and **8** also demonstrate significant potency against MCF-7 cells, with IC_{50} values of 4.17 and 27.73 μM, respectively.

Table 2.In vitro cytotoxic activity of certain synthetic compounds against tumor cell lines in contrast to Doxorubicin, a reference drug.

Compounds	In vitro Cytotoxicity IC_{50} (μM) •	
	HePG2	MCF7
DOX	**4.50±0.2**	**4.17±0.2**
7	**13.43±1.0**	**9.49±0.7**
4	**56.35±3.2**	**41.29±2.4**
8	**29.65±1.9**	**27.73±1.8**
1	**68.73±3.5**	**79.16±3.6**
6	**45.47±2.3**	**36.19±2.1**
5	**82.40±4.1**	**53.28±3.1**

• IC50 (μM): 1 – 10 (very strong). 11 – 20 (strong). 21 – 50 (moderate). 51 – 100 (weak) and above 100 (non-cytotoxic) •• DOX: Doxorubicin

_____

_____

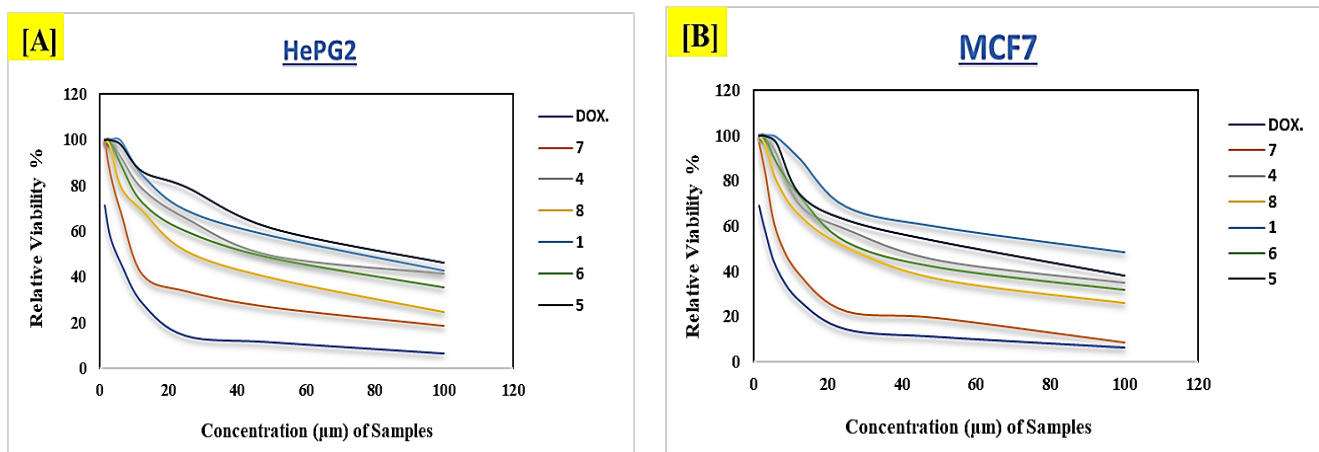### 3.4. Pharmacokinetics Studies

Figure 4: [A] Average of sample cell viability (%) for HEPG-2 and (B) Average of sample cell viability (%) for MCF-7.

POM analysis and other analogous processes are useful for determining a molecule's physicochemical qualities as well as predicting its biological activity, ADME parameters, and toxicity. The complex underwent a modified POM analysis with the MOLINSPIRATION tools. MOLINSPIRATION provides a full suite of computational biology programs to help with molecular manipulation and processing. These tools include SMILES and Sdfile conversion, molecule normalization, tautomer generation, molecule fragmentation, calculation of various molecular properties required for QSAR, molecular modeling and drug design, high-quality molecule depiction, and molecular database tools that assist in substructure and similarity searches [21, 42]. Table 3 illustrates the expected pharmacokinetic/Molinspiration properties of compounds 7 and 8. Using Molinspiration online screening, nearly all of the compounds generated show potential biological activity, as indicated by the docking parameters in Table 4, which highlight drug-like properties against kinase inhibitors, proteases, and enzyme inhibitors. The computed distribution of activity scores (version 2022.08) is compared to those for GPCR ligands, kinase inhibitors, ion channel modulators, nuclear receptor ligands, protease inhibitors, and other enzyme targets. These ratings provide scores for over 100,000 common drug-like compounds. From the results in Table 3, Compound 7 is more hydrophobic, smaller, lighter, and more flexible, perhaps making it more membrane-permeable yet less soluble in water but, Compound 8 is more hydrophilic, somewhat bigger, heavier, and less flexible, implying that it is better suited for interactions with polar environments like water, but may have lower membrane permeability.

Table 4 shows that Compound 7 is more effective as a GPCR ligand, nuclear receptor ligand, and protease inhibitor, making it ideal for signaling and protein breakdown inhibition while Compound 8 is more active as an ion channel modulator and kinase inhibitor, implying that it may be more effective at controlling ion flow and altering cellular signaling, particularly in cancer pathways. Compound 7 favors signaling and protease inhibition, but Compound 8 is better at ion channel modulation and kinase inhibition.

Table 3. Physicochemical properties of the compounds **7** and **8**

Compound	miLogP	TPSA	n-atoms	M.W.	n-ON	n-OHNH	n-violations	n-rotb	Volume
7	2.84	115.37	21	302.31	7	1	0	4	246.95
8	1.30	124.48	22	316.30	8	1	0	2	148.39

Abbreviations: Mi logP, the logarithm of partition coefficient of compound between n-octanol and water; MV, molecular volume; MW, molecular weight; n atoms, number of atoms; n-ON acceptors, number of hydrogen bond acceptors; n-OHNH donors, number of hydrogen bonds donors; n-rotb, number of routable bonds; n-violations, number of violations; TPSA, topological polar surface area.

_____

_____

Table 4. Physicochemical Molinspiration bioactivity score

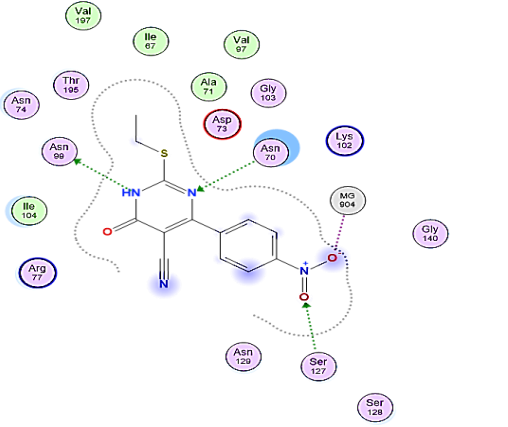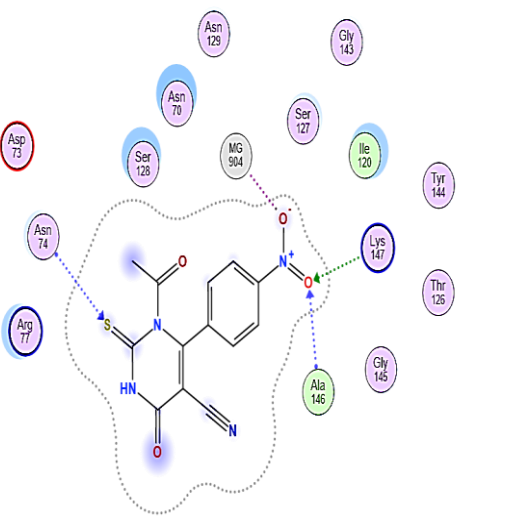| Compound	GPCR ligand	Ion channel modulator	Kinase inhibitor	Nuclear receptor ligand	Protease inhibitor	Enzyme inhibitor
7	-0.80	-0.62	-0.46	-0.70	-0.98	-0.36
8	-0.56	-0.91	-0.58	-0.54	-0.85	-0.30

3.5. Molecular docking simulation
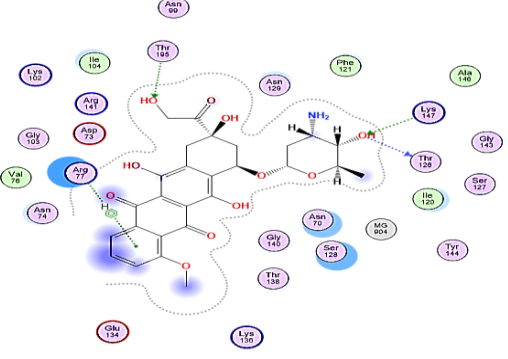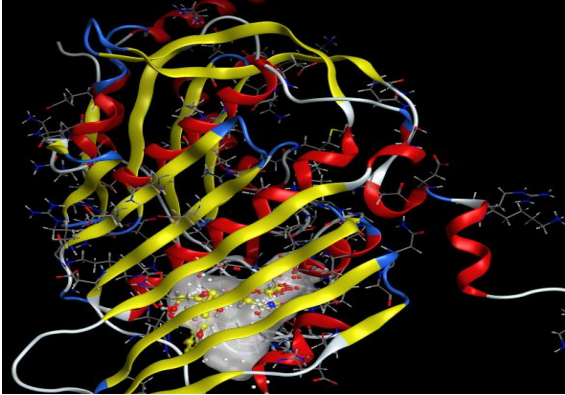
The enzyme Topoisomerase II enables the coiling and untangling of DNA, which is essential for the proliferation of cancer cells. This makes it a prime candidate for the development of potent anti-proliferative drugs[43].

In the Topoisomerase II binding site, newly synthesized molecules 7, 8, and 6 were docked, and their high-energy rating docking poses were recorded. Docking scores for compounds 7, 8, and 6 against doxorubicin at the HSP90 and Topoisomerase II enzyme binding sites are shown in Table 5. Compounds 7, 8, and 6 exhibit energy values of -7.19, -6.33, and -6.43 kcal/mol, respectively, in comparison to doxorubicin, which has an energy score of -7.42 kcal/mol. Figure 5a shows 2D and 3D representations of Doxorubicin, 7, 8, and 6 at the Topoisomerase II binding site (1QZR). Doxorubicin was selected as a reference compound in this study due to its extensive clinical application and proven efficacy against various types of human cancers, including hepatocellular carcinoma (HEPG-2) and breast cancer (MCF-7), which are the same cancer cell lines evaluated herein REF. It is a well-known anthracycline antibiotic that primarily exerts its cytotoxic activity through the inhibition of Topoisomerase II, making it highly relevant to the mechanistic targets explored in this work. Furthermore, its well-documented pharmacological profile and established binding characteristics with DNA and topoisomerase enzymes provide a reliable standard for evaluating and comparing the biological activity and docking performance of the newly synthesized pyrimidine derivatives. As was previously stated, HSP90 is an excellent candidate for the development of anti-proliferative drugs. Oncogenic proteins are degraded when HSP90 is inhibited, which is essential for the proliferation of cancer cells because it stops protein aggregation and ATP-dependent refolding[44]. According to reference[45], the HSP90 geldanamycin binding domain (PDB ID:1YET) was docked to the newly synthesized molecules 7, 8, and 6. Energy scores and docking poses were recorded for each compound (Table 5). In contrast to doxorubicin's energy score of -8.27 kcal/mol, compounds 7, 8, and 6 had energy scores of -6.28, -6.61, and -6.27 kcal/mol, respectively. Doxorubicin, **7**, **8**, and **6** at the HSP90 binding site (1YET) are shown in 2D and 3D in Figure 5b.

Table 5. MD scores and the amino acids involved in interactions for compounds **7, 8,** and **6** with the Topo II binding site (1QZR) and the HSP90 binding site (1YET) are compared to those of the reference ligand Doxorubicin.

Compounds	Topoisomerase II binding site (1QZR)		HSP90 binding site (1YET)	
	Docking score (Kcal/mol)	Amino acid H-bond (Bond length Ǻ)	Docking score (Kcal/mol)	Amino acid H-bond (Bond length Ǻ)
7	-7.19952011	ASN 99 (A) (3.46) ASN 70 (A) (3.45) SER 127 (A) (3.22) MG904 (A) (2.25)	-6.28592253	ASN 51 (A) (3.13)
8	-6.33586979	ALA 146 (A) (3.09) LYS 147 (A) (2.89) ASN 74 (A) (3.93) MG904 (A) (2.09)	-6.61420822	THR 184 (A) (3.01)
6	-6.43288136	ALA 146 (A) (3.28) LYS 147 (A) (3.04) MG904 (A) (2.09) SER 127 (A) (4.28) SER 128 (A) (3.68)	-6.27004385	GLY 97 (A) (3.17) THR 184 (A) (4.05)
Doxorubicin	-7.42926168	THR 126 (A) (2.90) THR195 (A) (3.02) LYS 147 (A) (3.16) ARG 77 (A) (4.26)	-8.27123833	ASP 54 (A) (3.28) GLY 97 (A) (3.05) LYS 58 (A) (3.02)

_____

Comp.	Two-dimensional representations	Three-dimensional representations
DOX.		
7		
8		

_____

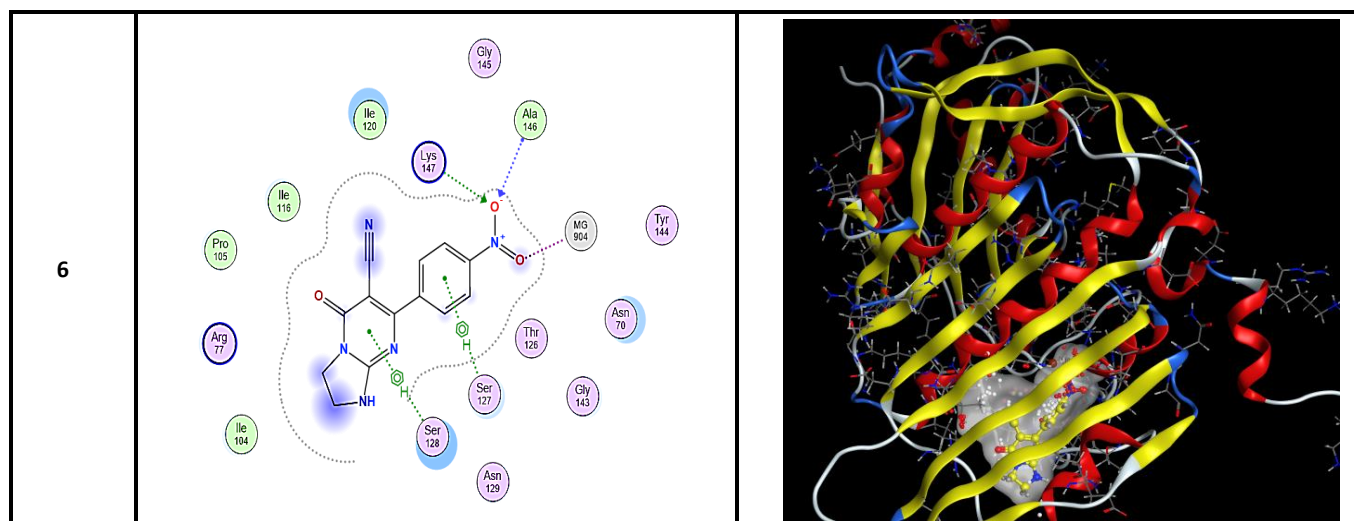*Egypt. J. Chem.* **68,** SI: Z. M. Nofal (2025)

| 6 | | |

Figure 5a. Two-dimensional (2D) presentations and alignment of compounds **8**, **7,** and **6** (Yellow) at the binding site of Topo II binding site (1QZR).

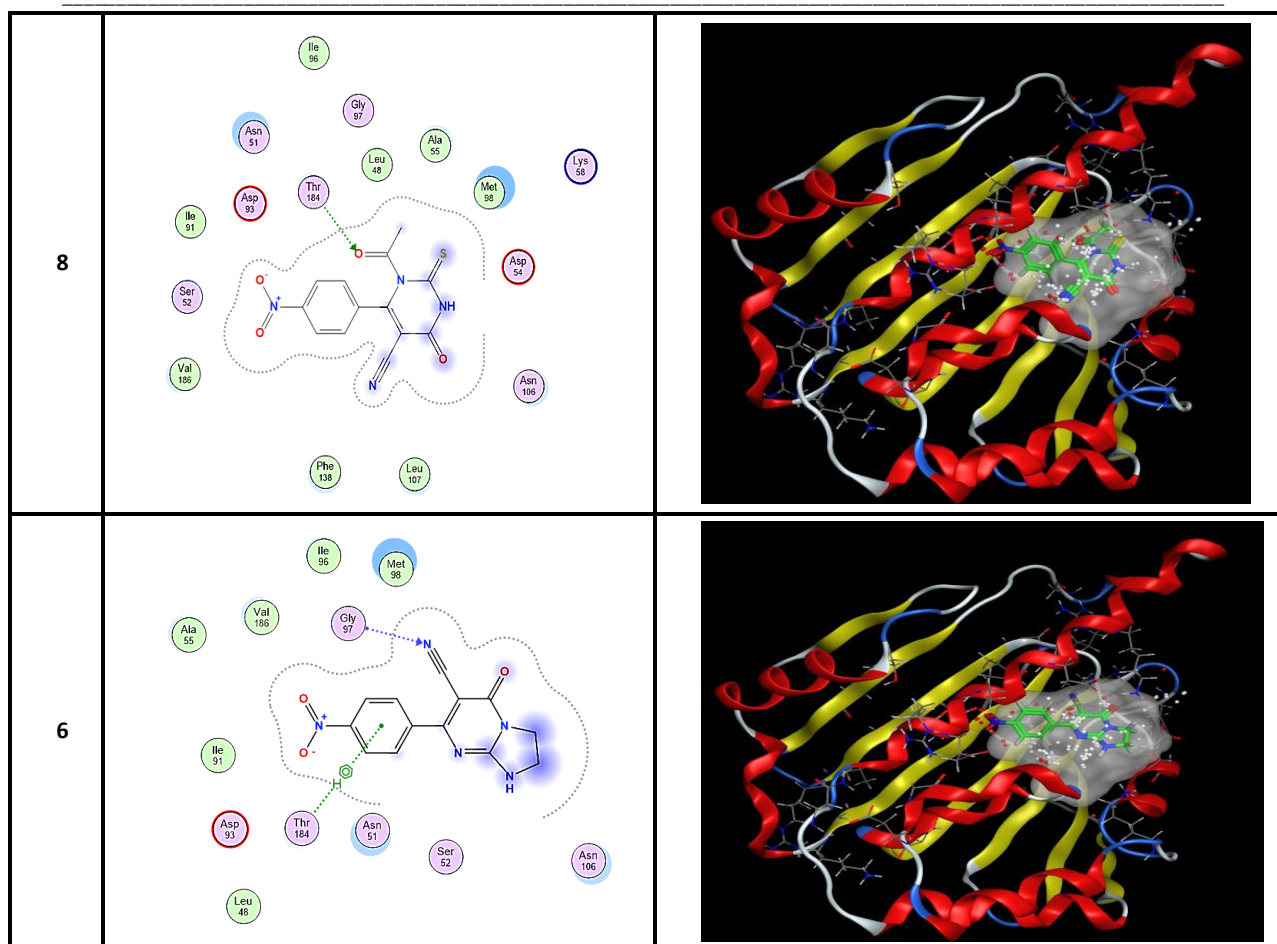| Comp.	Two-dimensional representations	Three-dimensional representations
DOX.		
7		

_____

Figure 5b. Two-dimensional (2D) presentations and alignment of compounds **7, 8,** and **6** (Green) at the binding site of HSP90 binding site (1YET)

4. Conclusion

This work effectively illustrated the use of Mn3O₄ nanoparticles as an effective and environmentally benign nano catalyst in the production of new pyrimidine derivatives. The necessary compounds were produced in good purity using the straightforward and efficient one-pot synthesis process. While biological analysis showed that some derivatives had potential anticancer activity against HePG2 and MCF7 cell lines with low damage on normal cells, structural characterization verified the production of the target molecules. Moreover, molecular docking research supported their potential as inhibitors of these important cancer targets by shedding light on the binding interactions with the enzymes Topoisomerase II and HSP90. All things considered, the combination of biological screening, computational modeling, green synthesis, and nano catalysis shows how promising these pyrimidine-based molecules are for future advancement in anticancer drug discovery.

Conflicts of interest: The authors declare that they have no competing interests.

References
1. Ganapathy, V., M. Thangaraju, and P.D. Prasad, *Nutrient transporters in cancer: relevance to Warburg hypothesis and beyond.* Pharmacology & therapeutics, 2009. **121**(1): p. 29-40.
2. Varmus, H., *The new era in cancer research.* Science, 2006. **312**(5777): p. 1162-1165.
3. Wang, Z., et al., *Synthesis, structure–activity relationships and preliminary antitumor evaluation of benzothiazole-2-thiol derivatives as novel apoptosis inducers.* Bioorganic & medicinal chemistry letters, 2011. **21**(4): p. 1097-1101.
4. Siegel, R.L., K.D. Miller, and A. Jemal, *Cancer statistics, 2018.* CA: a cancer journal for clinicians, 2018. **68**(1): p. 7-30.
5. Asham, H., et al., *Design, synthesis, and biological screening for cytotoxic activity of monastrol analogues.* Polycyclic Aromatic Compounds, 2022. **42**(8): p. 4863-4877.

_____

_____

6.   Mirzayi, S., et al., *Design and synthesis of tetrahydropyrimidinone (thione)-triazole hybrid scaffolds and evaluation of their biological activities.* Phosphorus, Sulfur, and Silicon and the Related Elements, 2021. **196**(12): p. 1109-1116.

7.   Ahangarzadeh, N., et al., *Design, synthesis, and in silico studies of tetrahydropyrimidine analogs as urease enzyme inhibitors.* Archiv der Pharmazie, 2022. **355**(10): p. 2200158.

8.   Flefel, E., et al., *A novel synthesis of some new pyrimidine and thiazolopyrimidine derivatives for anticancer evaluation.* Phosphorus, Sulfur, and Silicon and the Related Elements, 2007. **182**(8): p. 1739-1756.

9.   Rashad, A.E., et al., *New pyrimidinone and fused pyrimidinone derivatives as potential anticancer chemotherapeutics.* Archiv der Pharmazie, 2012. **345**(9): p. 729-738.

10.   Sepehri, S., H.P. Sanchez, and A. Fassihi, *Hantzsch-type dihydropyridines and biginelli-type tetra-hydropyrimidines: a review of their chemotherapeutic activities.* Journal of Pharmacy & Pharmaceutical Sciences, 2015. **18**(1): p. 1-52.

11.   Kantankar, A., et al., *Rational design, synthesis, biological evaluation and molecular docking studies of chromone-pyrimidine derivatives as potent anti-cancer agents.* Journal of Molecular Structure, 2021. **1239**: p. 130502.

12.   Milović, E., et al., *Synthesis, characterization, and biological evaluation of tetrahydropyrimidines: Dual-activity and mechanism of action.* Pharmaceutics, 2022. **14**(10): p. 2254.

13.   Razzaghi-Asl, N., et al., *Design, synthesis and evaluation of cytotoxic, antimicrobial, and anti-HIV-1 activities of new 1, 2, 3, 4-tetrahydropyrimidine derivatives.* Research in Pharmaceutical Sciences, 2019. **14**(2): p. 155-166.

14.   Safari, S., et al., *Synthesis, biological evaluation and molecular docking study of dihydropyrimidine derivatives as potential anticancer agents.* Journal of Heterocyclic Chemistry, 2020. **57**(3): p. 1023-1033.

15.   Nafie, M.S., et al., *Discovery of novel pyrazolo [3, 4-b] pyridine scaffold-based derivatives as potential PIM-1 kinase inhibitors in breast cancer MCF-7 cells.* Bioorganic & Medicinal Chemistry, 2020. **28**(24): p. 115828.

16.   Tantawy, E.S., et al., *Synthesis, characterization of some pyrazine derivatives as anti-cancer agents: In vitro and in Silico approaches.* Journal of Molecular Structure, 2020. **1210**: p. 128013.

17.   Ramadan, S.K., E.A. El-Helw, and H.A. Sallam, *Cytotoxic and antimicrobial activities of some novel heterocycles employing 6-(1, 3-diphenyl-1 H-pyrazol-4-yl)-4-oxo-2-thioxo-1, 2, 3, 4-tetrahydropyrimidine-5-carbonitrile.* Heterocyclic communications, 2019. **25**(1): p. 107-115.

18.   Patil, T.P., et al., *Green synthesis of gold nanoparticles via Capsicum annum fruit extract: characterization, antiangiogenic, antioxidant and anti-inflammatory activities.* Applied Surface Science Advances, 2023. **13**: p. 100372.

19.   Elsayed, D.A., et al., *TiO2 nanoparticle as catalyst for an efficient green one-pot synthesis of 1H-3-Indolyl Derivatives as significant antiviral activity.* Bioorganic Chemistry, 2022. **124**: p. 105805.

20.   Shehab, W.S., et al., *Pharmacokinetic and molecular docking studies to pyrimidine drug using Mn3O4 nanoparticles to explore potential anti-Alzheimer activity.* Scientific Reports, 2024. **14**(1): p. 15436.

21.   Shehab, W.S., et al., *CuO nanoparticles for green synthesis of significant anti-Helicobacter pylori compounds with in silico studies.* Scientific Reports, 2024. **14**(1): p. 1608.

22.   Hamed, E.O., et al., *Cyclization of N-acetyl derivative: Novel synthesis–azoles and azines, antimicrobial activities, and computational studies.* Heterocyclic Communications, 2022. **28**(1): p. 35-43.

23.   El-Kalyoubi, S., et al., *Synthesis, DFT calculations, and anti-proliferative evaluation of pyrimidine and selenadiazolopyrimidine derivatives as dual Topoisomerase II and HSP90 inhibitors.* Journal of Enzyme Inhibition and Medicinal Chemistry, 2023. **38**(1): p. 2198163.

24.   Elsayed, D.A., *Design, synthesis, biological evaluation, and molecular docking studies of novel azo-compounds derivatives as significant antioxidants.* Bulletin of Faculty of Science, Zagazig University, 2023. **2023**(1): p. 1-9.

25.   Abd El Hadi, S.R., et al., *Unravelling the potency of the 4-oxo-2-thioxo-1, 2, 3, 4-tetrahydropyrimidine-5-carbonitrile scaffold with S-arylamide hybrids as PIM-1 kinase inhibitors: synthesis, biological activity and in silico studies.* RSC Medicinal Chemistry, 2025.

26.   Abdelhameed, R.M., et al., *Novel triazolothiadiazole and triazolothiadiazine derivatives containing pyridine moiety: design, synthesis, bactericidal and fungicidal activities.* Current Bioactive Compounds, 2018. **14**(2): p. 169-179.

27.   Elsayed, D.A., et al. *A Concise Review of Nanocomposites' Function in Organic Reactions to Synthesize Various Organic Nuclei.* 2024. International Exchange and Innovation Conference on Engineering & Sciences.

28.   Abdo, S.M., et al., *Sustainable Development of Antimicrobial Polyvinyl Chloride Bioplastics Using Chlamydomonas reinhardtii Extract.* Egyptian Journal of Chemistry, 2025. **68**(8): p. 77-96.

29.   Shehab, W.S., et al., *Design, Synthesis and Characterization of New Fused Pyrazole Systems: In Vitro Anti-bacterial, Anti-fungal, Antioxidant Evaluation, In Silico DFT and Molecular Docking Studies.* Journal of Molecular Structure, 2025: p. 142163.

30.   Gad, M., et al., *Sustainable Production of Lactic Acid by Enterococcus Gallinarum from Agricultural Wastes.* Egyptian Journal of Chemistry, 2025. **68**(7): p. 17-31.

31.   Prodromou, C., *Mechanisms of Hsp90 regulation.* Biochemical Journal, 2016. **473**(16): p. 2439-2452.

32.   Mosmann, T., *Rapid colorimetric assay for cellular growth and survival: application to proliferation and cytotoxicity assays.* Journal of immunological methods, 1983. **65**(1-2): p. 55-63.

33.   Lappalainen, K., et al., *Comparison of cell proliferation and toxicity assays using two cationic liposomes.* Pharmaceutical research, 1994. **11**: p. 1127-1131.

_____

_____

34.   Rizvi, S.M.D., S. Shakil, and M. Haneef, *A simple click by click protocol to perform docking: AutoDock 4.2 made easy for non-bioinformaticians.* EXCLI journal, 2013. **12**: p. 831.

35.   Classen, S., S. Olland, and J.M. Berger, *Structure of the topoisomerase II ATPase region and its mechanism of inhibition by the chemotherapeutic agent ICRF-187.* Proceedings of the national academy of sciences, 2003. **100**(19): p. 10629-10634.

36.   Stebbins, C.E., et al., *Crystal structure of an Hsp90–geldanamycin complex: targeting of a protein chaperone by an antitumor agent.* Cell, 1997. **89**(2): p. 239-250.

37.   El-Kalyoubi, S., et al., *Novel Aminopyrimidine-2, 4-diones, 2-Thiopyrimidine-4-ones, and 6-Arylpteridines as Dual-Target Inhibitors of BRD4/PLK1: Design, Synthesis, Cytotoxicity, and Computational Studies.* Pharmaceuticals, 2023. **16**(9): p. 1303.

38.   Apte, S., et al., *Nanosize Mn3O4 (Hausmannite) by microwave irradiation method.* Materials Research Bulletin, 2006. **41**(3): p. 647-654.

39.   Seo, W.S., et al., *Size-dependent magnetic properties of colloidal Mn3O4 and MnO nanoparticles.* Angewandte Chemie International Edition, 2004. **43**(9): p. 1115-1117.

40.   Raj, B.G.S., et al., *Synthesis of Mn3O4 nanoparticles via chemical precipitation approach for supercapacitor application.* Journal of Alloys and Compounds, 2015. **636**: p. 234-240.

41.   Ramadan, S.K., E.A.E. El-Helw, and H.A. Sallam, *Cytotoxic and antimicrobial activities of some novel heterocycles employing 6-(1,3-diphenyl-1H-pyrazol-4-yl)-4-oxo-2-thioxo-1,2,3,4-tetrahydropyrimidine-5-carbonitrile.* Heterocyclic Communications, 2019. **25**(1): p. 107-115.

42.   Kashyap, A., et al., *Microwave-assisted synthesis of hybrid PABA-1, 3, 5-triazine derivatives as an antimalarial agent.* Journal of Biochemical and Molecular Toxicology, 2021. **35**(9): p. e22860.

43.   Sordet, O., et al., *Apoptosis induced by topoisomerase inhibitors.* Current Medicinal Chemistry-Anti-Cancer Agents, 2003. **3**(4): p. 271-290.

44.   Hong, T.-J., et al., *Identification of new Hsp90 inhibitors by structure-based virtual screening.* Bioorganic & medicinal chemistry letters, 2009. **19**(16): p. 4839-4842.

45.   Challan, S., S. Khater, and A. Rashad, *Preparation, molecular modeling and in-vivo evaluation of 99mTc-Oseltamivir as a tumor diagnostic agent.* International Journal of Radiation Research, 2022. **20**(3): p. 635-642.

_____